HHS Public Access

Author manuscript

Adv Genet. Author manuscript; available in PMC 2016 June 25.

Published in final edited form as:

Adv Genet. 2010 ; 69: 1–30. doi:10.1016/S0065-2660(10)69010-4.

MR Molecular Imaging of Tumor Vasculature and Vascular Targets

Arvind P. Pathak[*,†], **Marie-France Penet**[*], and **Zaver M. Bhujwalla**[*,†]

[*]JHU ICMIC Program, Russell H. Morgan Department of Radiology and Radiological Science, The Johns Hopkins University School of Medicine, Baltimore, Maryland, USA

[†]The Sidney Kimmel Comprehensive Cancer Center, The Johns Hopkins University School of Medicine, Baltimore, Maryland, USA

Abstract

Tumor angiogenesis and the ability of cancer cells to induce neovasculature continue to be a fascinating area of research. As the delivery network that provides substrates and nutrients, as well as chemotherapeutic agents to cancer cells, but allows cancer cells to disseminate, the tumor vasculature is richly primed with targets and mechanisms that can be exploited for cancer cure or control. The spatial and temporal heterogeneity of tumor vasculature, and the heterogeneity of response to targeting, make noninvasive imaging essential for understanding the mechanisms of tumor angiogenesis, tracking vascular targeting, and detecting the efficacy of antiangiogenic therapies. With its noninvasive characteristics, exquisite spatial resolution and range of applications, magnetic resonance imaging (MRI) techniques have provided a wealth of functional and molecular information on tumor vasculature in applications spanning from “bench to bedside”. The integration of molecular biology and chemistry to design novel imaging probes ensures the continued evolution of the molecular capabilities of MRI. In this review, we have focused on developments in the characterization of tumor vasculature with functional and molecular MRI.

I. INTRODUCTION

The two major mechanisms resulting in the formation of blood vessels are vasculogenesis and angiogenesis. Vasculogenesis describes the establishment of the vasculature during embryogenesis and development. Angiogenesis, a term coined by Dr. John Hunter in 1794 to describe the formation of new blood vessels from extant vasculature (Hunter, 1794), is a process that occurs in both the embryo and the adult (Carmeliet, 2005). In 1865, Rudolf Virchow made the observation that tumors have distinct capillary networks (Virchow, 1863), which was followed by the first systematic studies of the tumor vasculature by Goldman in 1907 (Goldman, 1907) and by Lewis in 1927 who determined that the tumor environment has a profound effect on the architecture of angiogenic vessels (Lewis, 1927). (See Ribatti's (2009) comprehensive treatise on the history of tumor angiogenesis research.) A century later, the observation that adult angiogenesis was a hallmark of pathologies ranging from cancer to diabetic retinopathy (Jain and Carmeliet, 2001) led Folkman (1971) to posit in his seminal paper that solid tumor growth was “angiogenesis-dependent”. In it, he also introduced the concept of “antiangiogenic” therapy or the idea that solid tumor growth could

be arrested by preventing the recruitment and formation of de novo blood vessels. In the decades since, a comprehensive understanding of the molecular mechanisms regulating tumor angiogenesis has emerged, resulting in the identification of a slew of angiogenesis inhibitors, many of which are currently in clinical trials (Folkman, 2007).

In a careful study of carcinoma of the bronchus, Thomlinson and Gray observed that the onset of necrosis occurred at approximately 160 μm from the nearest vessel, a distance calculated to be the diffusion limit of oxygen. Based on these data, they predicted the presence of hypoxia in tumors that would lead to radioresistance (Thomlinson and Gray, 1955). Almost four decades later, with the discovery of the hypoxia inducible factor-1 (HIF-1), and its role as a transcriptional regulator of an ever-increasing list of genes (Semenza, 2010), tumor hypoxia resulting from the chaotic tumor vasculature has been implicated in metabolism, angiogenesis, invasion, metastasis, and drug resistance (Bertout *et al.*, 2008).

Since Clark *et al.* (1931) created some of the earliest images of neovascularization in transparent rabbit ear chambers in the 1930s, advances in physics (e.g., new imaging methods), chemistry (e.g., the synthesis of novel imaging probes), and biology (e.g., development of innovative gene reporter systems and the identification of novel targets) have ushered in a new era in the characterization of angiogenesis and antiangiogenic therapy using imaging (McDonald and Choyke, 2003; Pathak *et al.*, 2008a). Even a century ago, the importance of “individualizing cancer treatment” and “penetrating into the darkness of physiological conditions existing in tumor growths” was recognized in the prescient remarks made by E. Goldman in 1907 (Goldman, 1907).

The importance of tumor vasculature in several phenotypic characteristics of cancer, as well as in drug delivery and metastasis, has become very evident, and angiogenic or vascular targeting is meeting with some success as a potential treatment for cancer (Folkman, 2007; Neri and Bicknell, 2005). These developments have not only necessitated the genomic and functional characterization of individual tumors to identify specific molecular targets, but also the ability to noninvasively detect the spatial and temporal response to these new targeted therapies. Noninvasive imaging techniques, the availability of “smart probes” as well as molecular strategies such as the use of small interfering RNA to downregulate specific targets are playing an increasingly important role in this era of targeted molecular medicine. The purpose of this review is to describe recent advances in MRI as applied to tumor vasculature characterization and targeting.

II. STRUCTURAL, FUNCTIONAL, AND MOLECULAR CHARACTERISTICS OF TUMOR VASCULATURE

Studies of tumor vascular morphology have identified a variety of structural and functional differences between tumor and normal vasculature (see Konerding *et al.*, 2000 for a comprehensive review). Tumor-induced blood vessels are typically sinusoidal, exhibit discontinuous basement membranes, and lack tight endothelial cell junctions making them highly permeable to macromolecules. Other characteristics of the tumor vasculature include (i) spatial heterogeneity and loss of branching hierarchy, (ii) arteriovenous shunts, (iii)

acutely and transiently collapsing vessels, (iv) poor differentiation and a lack of smooth muscle cell lining, and (v) an inability to match the elevated metabolic demand of cancer cells, resulting in areas of hypoxia and necrosis.

Pioneering work by Jain, Vaupel, and others has demonstrated that structural anomalies of the tumor vasculature result in altered hemodynamics, blood rheology, and tumor blood flow (Jain, 1988; Vaupel *et al.*, 1989). Figure 1.1 summarizes the bidirectional relationships between the anomalous aspects of the tumor vasculature and the resulting pathophysiological and molecular perturbations in the tumor microenvironment.

In addition to angiogenesis-dependent pathways, nonangiogenic pathways for tumor growth have also been observed. Of these, vascular cooption and vasculogenic mimicry are the most well known. In a landmark study, Holash *et al.*, (1999) demonstrated that in contrast to the prevailing view that most tumors begin as avascular masses, a subset of tumors initially grew by “coopting” existing host blood vessels. This coopted host vasculature did not immediately undergo angiogenesis but initially regressed, leading to an avascular tumor with massive tumor cell loss. Eventually, the remaining tumor was rescued by robust angiogenesis at the tumor rim. Maniotis *et al.* (1999) described another mode of vascular channel formation which was dubbed “vasculogenic mimicry” to highlight the fact that parts of the microcirculation of aggressive uveal melanomas consist of channels lined by a layer of extracellular matrix and the tumor cells themselves. Chang *et al.* (2000) have described the formation of “mosaic vessels” in a colon carcinoma model, wherein both tumor and endothelial cells contributed to vascular tube formation.

The heterogeneity of tumor vasculature can pose a formidable clinical challenge. The structural and functional deficiencies of the tumor vasculature profoundly impact drug delivery, radiosensitivity, proliferation rate, invasion, metastases, and the metabolic micromilieu (pO2, pH, energy status; Konerding *et al.*, 2000) of the tumor. However, as discussed subsequently, this heterogeneity of the tumor vasculature also presents an opportunity for the identification of novel drug targets that can be exploited to develop tumor vasculature-selective therapeutic strategies (Neri and Bicknell, 2005).

As summarized in several excellent reviews (Baluk *et al.*, 2005; McDonald and Choyke, 2003; Munn, 2003), the physiology and organization of the tumor vasculature at the spatial scale of the endothelial cell is also abnormal. Such abnormalities include gaps in interendothelial tight junctions resulting in loss of barrier function, loose or no association with pericytes, and a compromised or incomplete basement membrane (Kalluri, 2003). This microscopic picture is further complicated by the phenomena of vasculogenic mimicry and mosaic vessels described earlier. However, at this scale, the diversity of surface proteins selectively expressed by angiogenic tumor vessels has been exploited as targets for novel contrast agents using a range of imaging modalities (McDonald and Choyke, 2003). Some of these epitopes on angiogenic endothelial cells and basement membrane components have also been tested for tumor vessel selective drug-targeting strategies as summarized in Table 1.1 (Molema, 2005). The review by Langenkamp and Molema (2009) lists endothelial cell-specific genes used to identify tissue microvasculature, while a landmark paper by Croix *et al.* (2000) demonstrates the diversity of the genes expressed in human tumor endothelium.

Both imaging receptor expression and vascular targeting are discussed in detail in ensuing sections.

Conventional image contrast in radiologic images provides differences in the level of brightness or intensity of parts of the image corresponding to anatomically or physiologically different locations. While traditionally such contrast has aided in the differentiation of normal from pathologic tissue, such images provide little information regarding the functional or molecular status of a lesion. For example, one cannot infer the angiogenic status of the tumor vasculature from conventional imaging (Pathak *et al.*, 2008a). A wide array of noninvasive imaging modalities has been used to image the tumor vasculature. These include X-ray computed tomography (CT), MRI, positron emission tomography (PET), single-photon emission computed tomography (SPECT), ultrasound, and different types of optical imaging, each with its own distinct advantages as a tool in the noninvasive, in vivo assessment of tumor angiogenesis (Glunde *et al.*, 2007). However, the assortment of available “functional” contrast mechanisms in conjunction with the development of novel imaging probes is making MRI a valuable imaging modality for the functional and molecular imaging of tumor vasculature in vivo. Here we have outlined the diversity and utility of MRI and provided brief descriptions of the biophysical phenomena underlying some of the contrast mechanisms used in MRI of tumor vasculature.

III. BASIS OF CONTRAST IN MR IMAGES

Almost every contrast mechanism for probing the tumor vasculature, including the use of exogenous MR contrast agents and targeted probes, in some way results from changes in the MR signal intensity brought about by changes in what are collectively known as tissue “relaxation times” (T_1 and T_2, or T_2^*). Briefly, the spin-lattice or longitudinal relaxation time (T_1) is the time constant that characterizes the exponential process by which the longitudinal component of the tissue magnetization returns or “relaxes” to its equilibrium value. It does so by exchanging energy with its surroundings or lattice, at the Larmor frequency ($\omega_0=\gamma B_0$, where ω_0 is the rate of precession of the ensemble of spins under the influence of an applied magnetic field B_0 and γ is the gyromagnetic ratio). At the molecular scale, T_1 relaxation occurs through interactions between protons in tissue water and those on macromolecules or proteins, and by interactions with paramagnetic substances, that is, substances with unpaired electrons in their outermost shells. T_1-based MR contrast results from differences in T_1 dominating the signal intensity in the MR image. Tissues with short T_1s (such as fat) appear bright in T_1-weighted MRI, since the longitudinal magnetization recovers to equilibrium rapidly relative to tissues with long T_1s (such as cerebrospinal fluid).

Microscopic magnetic field heterogeneities in the applied magnetic field of an MRI scanner, as well as variations in local magnetic susceptibility due to the physiological microenvironment, cause spins contributing to the transverse component of the tissue magnetization, to lose phase coherence. The process through which this occurs is known as T_2^* relaxation. The loss in phase coherence attributable to static magnetic field heterogeneities can be recovered using a refocusing radiofrequency (RF) pulse or a spin-echo (SE) imaging method. However, as protons diffuse through the microscopic field inhomogeneities, they also lose phase coherence due to Brownian motion through these

microscopic magnetic field gradients, which results in a phase dispersion that cannot be reversed by the application of a refocusing pulse. This is known as T_2 relaxation and in T_2-weighted MR images, tissues with short T_2s, such as the liver, appear dark due to the rapid decay of transverse magnetization compared to those with long T_2s, such as fat. Similarly, in T_2^*-weighted images, regions with large susceptibility gradients such as air–tissue interfaces of the orbits of the eye, or large veins carrying deoxygenated blood, appear hypointense. A computational model illustrating the T_2^* contrast mechanism is shown in Fig. 1.2 (Pathak *et al.*, 2008b). Figure 1.2A is a volume rendering of a contrast agent bearing cerebrocortical capillary network from a rat brain, which results in a susceptibility gradient relative to the surrounding tissue. This susceptibility gradient in turn, perturbs the applied magnetic field at the microscopic scale as illustrated in Fig. 1.2B. Finally, water protons diffusing through these microscopic magnetic field heterogeneities experience different phase shifts resulting in a loss of phase coherence and attenuation of the MRI signal. An example of these diffusion trajectories is illustrated in Fig. 1.2C for the case of a single contrast agent bearing capillary.

A. Endogenous contrast

Probing tumor vasculature using the inherent or endogenous contrast produced by deoxyhemoglobin in tumor microvessels is based on the blood oxygenation level dependent (BOLD) contrast mechanism discovered by Ogawa (1990). The primary determinant of the MRI contrast observed is the concentration of paramagnetic deoxyhemoglobin. The presence of deoxyhemoglobin in a blood vessel causes a susceptibility difference between the microvessel and the surrounding tissue inducing microscopic magnetic field gradients that cause dephasing of the MR signal, leading to a reduction in the value of T_2^*. Since oxyhemoglobin is diamagnetic and does not produce the same dephasing, changes in blood oxygenation are observable as signal changes in T_2^*-weighted images. The dependence of T_2^* on oxygenation in a tissue can be approximated as

$$\frac{1}{T_2^*} \propto (1 - Y)\, b \qquad (1.1)$$

where Y is the fraction of oxygenated blood and b the fractional blood volume. In hypoxic tumors where 0<Y<0.2, BOLD contrast is primarily dependent on b. This method works best in poorly oxygenated tumors and human xenografts with randomly oriented angiogenic microvessels. While this approach provides a fast and noninvasive measurement of tumor fractional blood volume without requiring the administration of an exogenous contrast, it does not provide quantitative assessment of tumor vascular volume, vascular permeability, or blood flow. Nonetheless, BOLD MRI has been used to detect changes in tumor oxygenation following induction of angiogenesis (Abramovitch *et al.*, 1999), to obtain maps of the “functional” vasculature in genetically modified HIF-1 (+/+ and −/−) models (Carmeliet *et al.*, 1998), and was recently shown to correlate with mean tumor pO2 measured using fluorine-19 [19F] MRI oximetry (Zhao *et al.*, 2009). It is important to bear in mind that the relationship between angiogenesis and BOLD image contrast is complex as it is not solely determined by the oxygenation status of blood, but is also affected by factors such as oxygen

saturation, hematocrit, blood flow, blood volume, vessel orientation, and geometry (Pathak *et al.*, 2003).

In 2000, Silva *et al.* demonstrated the feasibility of imaging blood flow in a rodent brain tumor model, using another endogenous contrast MR mechanism known as arterial spin labeling (ASL) (Silva *et al.*, 2000). In this approach, arterial blood water serves as the endogenous tracer, and is magnetically tagged proximal to the brain, using spatially selective RF inversion pulses. The effect of arterial tagging on downstream images can then be quantified in terms of tissue blood flow, since changes in signal intensity depend on the regional blood flow and degree of T_1 relaxation. Tissue blood flow images can then be computed from tagged and untagged control images. Although ASL exhibits sufficient sensitivity at high magnetic fields for mapping the tumor blood flow, it may not perform as well when blood flow in tumor vessels is very low, since the tagged arterial blood may not reach the tissue in time, relative to their T_1 relaxation time, that is, the spins will be fully relaxed by the time they enter the imaging volume. Recent studies have demonstrated excellent correlation between ASL and dynamic susceptibility contrast (DSC) MRI-derived measures of blood flow in patients with brain tumors, further establishing the utility and validity of ASL (Jarnum *et al.*, 2010; Knutsson *et al.*, 2010).

The advantage of characterizing the tumor vasculature with endogenous contrast-based MRI is that it does not require the intravenous (i.v.) administration of a contrast agent, making it entirely noninvasive, providing dynamic data with high temporal resolution. Repeated measurements in preclinical studies are therefore only limited by the constraints of anesthesia. However, using such approaches, one cannot quantify physiologic parameters like the tumor vascular volume or vascular permeability, which require the administration of exogenous MRI contrast agents.

B. Exogenous contrast

Unlike the dyes or tracers employed with nuclear medicine, X-ray or optical imaging techniques, MR contrast agents are not visualized directly in an MR image, but indirectly by the changes they induce in water proton relaxation behavior. The most commonly used MR contrast agents are paramagnetic gadolinium chelates. These agents are tightly bound complexes of the element gadolinium (Gd) and various chelating agents (Lauffer, 1987). The seven unpaired electrons of gadolinium produce a large magnetic moment that shortens both T_1 and T_2 of tissue water. Since tissue T_2 values are intrinsically shorter than the corresponding T_1 values, the T_1 effect of the contrast agent dominates, and tissues that take up the agent are brightened in T_1-weighted images. The magnetic susceptibility differences induced by Gd-based contrast agents shorten the T_2 and T_2^* of tissue water and tissues that take up the paramagnetic agent are darkened in T_2- and T_2^*-weighted images. A range of vascular parameters can be calculated from tracer kinetics principles, using the tissue concentration of Gd-based agents (Zaharchuk, 2007).

Gd-based complexes may be broadly classified as either being low molecular weight (≈0.57 kDa) agents, for example, gadolinium diethylenetriamine pentaacetic acid (GdDTPA) compounds used clinically for contrast enhancement of malignant tumors, or

macromolecular agents (≈90 kDa) such as albumin-GdDTPA, that are confined to the vascular compartment for several hours and are used in preclinical studies of tumor angiogenesis. MR methods used to characterize tumor vascularization depend on the physical properties and pharmacokinetics of the contrast agent used (Fig. 1.3). A brief overview of some of these methods is presented in the subsequent sections.

C. Low molecular weight contrast agents

Several compounds in this class of paramagnetic agents are approved for routine clinical use and have been used to characterize the vasculature in a variety of tumors, including breast (Baar *et al.*, 2009), brain (Batchelor *et al.*, 2007), and cervical tumors (Mayr *et al.*, 2010). Most T_1 methods involve the analyses of relaxivity changes induced by the contrast agent to determine influx and outflux transfer constants, as well as the extracellular extravascular volume fraction based on one of several compartmental models (Fig. 1.3A; Tofts, 1997). Although not freely diffusible, this class of agent remains in the extracellular space, and three standard kinetic parameters can be derived from dynamic contrast-enhanced (DCE) T_1-weighted MRI: (i) K_{trans} (min^{-1}), which is the volume transfer constant between the blood plasma and the extravascular extracellular space (EES); (ii) k_{ep} (min^{-1}), which is the rate constant between the EES and blood plasma; and (iii) v_e (%), which is the volume of the EES per unit volume of tissue, that is, the volume fraction of the EES (Tofts, 1997). k_{ep} can be derived from the shape of the tracer concentration–time curve, but the determination of K_{trans} requires absolute values of the tracer concentration. K_{trans} has several different connotations depending on the balance between blood flow (F) and capillary permeability (P) in the tissue of interest. For example, in most tumors the leakage concentration is limited by the flow-rate. Thus, in this flow-limited or high-permeability regime, solving the differential equation that relates tissue concentration (C_t) to the plasma concentration (C_p) yields: $K_{trans}=F\rho(1–Hct)$, where F (ml g^{-1} min^{-1}) is the flow of whole blood per unit mass of tissue, ρ is the tissue density (g ml^{-1}), Hct the hematocrit, and (1–Hct) the plasma fraction. An excellent review of DCE MRI tracer kinetic models, terminology, and definitions can be found in Tofts *et al.* (1999). To calculate K_{trans} and $_{ve}$, the plasma and tissue concentrations of the contrast agent are required. Typically the plasma concentration (also known as the arterial input function, AIF) can be measured using voxels localized within a large blood vessel or approximated by a biexponential curve (Ohno *et al.*, 1979). In most DCE MRI models, the concentration of GdDTPA is measured from changes in the T_1 relaxation rate, assuming that water is in fast exchange between the vascular and extracellular compartments. It has been demonstrated by several investigators that the accuracy of DCE MRI-derived vascular volumes can be significantly affected by incorrect assumptions regarding exchange rates (Donahue *et al.*, 1997; Kim *et al.*, 2002; Landis *et al.*, 2000).

As mentioned earlier, low molecular weight Gd-chelates employed in MRI produce both T_1 and T_2 relaxation effects. However, when high doses of these agents are employed, the induced bulk susceptibility differences between the intra- and extravascular spaces dominate classical dipole–dipole relaxation. MRI contrast can be engendered from local magnetic field heterogeneities either by proton diffusion through the microscopic field inhomogeneities or via intravoxel dephasing. In the latter mechanism, the presence of

microscopic field inhomogeneities within an imaging voxel produces a heterogeneity of resonant frequencies which affects the MR signal intensity even in the absence of diffusion. The effect of magnetic field inhomogeneities on transverse relaxation can be summarized as (Fisel *et al.*, 1991; Kennan, 1994):

$$\frac{1}{T_2^*}=\frac{1}{T_2}+\frac{1}{T'_2} \quad (1.2)$$

The relaxation rate $1/T_2^*$ (R_2^*) is the rate of free induction decay or the rate at which the gradient-echo (GE) amplitude decays. The relaxation rate $1/T_2$(R2) is the rate at which the spin-echo (SE) amplitude decays. The relaxation rate, $1/T_2^{'}$ $\left(R_2^{'}\right)$, is the water resonance line-width, which is a measure of the frequency distribution within a voxel. In the presence of a contrast agent bearing tumor vessel, the relative R2 and R_2^* relaxation rates depend on the diffusion coefficient (D) of spins in the vicinity of the induced magnetic field inhomogeneities, radius (R) of the tumor vessel, and the variation of the Larmor frequency (dω) at the surface of the vessel (Fisel *et al.*, 1991; Kennan, 1994; Weisskoff *et al.*, 1994; Yablonskiy, 1994). The relationship between the two physical characteristics (R and D) can be described in terms of the proton correlation time τ_D:

$$\tau_{\mathrm{D}}=\frac{R^2}{D} \quad (1.3)$$

Depending on the relative magnitudes of dω and τ_D, the magnitude of susceptibility-induced relaxation effects is divided into three regimes (Fisel *et al.*, 1991; Kennan, 1994; Villringer *et al.*, 1988; Weisskoff *et al.*, 1994; Yablonskiy, 1994).

- **(i)** Fast exchange regime—in this regime, the rate of diffusion ($1/\tau_D$) is substantially greater than the frequency variation (dω), that is, τ_D dω≪1. This is known as the "motionally narrowed" regime as the susceptibility-induced local magnetic field gradients are averaged out (Boxerman *et al.*, 1995; Fisel *et al.*, 1991; Kennan, 1994).
- **(ii)** Slow exchange regime—in this regime, the rate of diffusion (1 τ_D) is substantially smaller than the frequency variation (dω), that is, τ_D dω≫1. Thus, the phase that a proton accumulates as it passes one perturber is large, that is, the effect is the same as it would be for the case of static field inhomogeneities. There is no signal attenuation on a T_2-weighted scan because the 180° RF pulse during the SE sequence refocuses static magnetic field inhomogeneities, while intravoxel dephasing still occurs in a GE sequence.
- **(iii)** Intermediate exchange regime—in this regime, τ_D dω~1, that is, water diffusion is neither fast enough to be fully motionally narrowed nor slow enough to be approximated as linear gradients, making the description of the susceptibility-induced contrast more complex. In this regime, analytic solutions to estimate signal loss in the presence of diffusion becomes complicated due to the large spatial

heterogeneity of the induced field gradients and numerical simulations are required (Boxerman *et al.*, 1995; Kennan, 1994; Weisskoff *et al.*, 1994).

A consequence of these regimes is that the SE and GEMRI methods have greatly different sensitivities to the size and scale of the field inhomogeneities, resulting in a differential sensitivity to contrast agent bearing tumor vessel caliber. It has been shown that the SE relaxation rate change (ΔR_2) increases, peaks for capillary-sized vessels (5–10 μm), and then decreases inversely with vessel radius, while the GE relaxation rate change (ΔR_2^*) increases and then plateaus to remain independent of vessel radius beyond capillary-sized vessels (Boxerman *et al.*, 1995; Weisskoff *et al.*, 1994). Therefore, SE methods are maximally sensitive to the microvascular blood volume, while the GE methods are more sensitive to the total blood volume. Based on this observation, SE sequences have been used in many tumor studies with the assumption that tumor angiogenesis is primarily characterized by an increase in the microvasculature (Aronen *et al.*, 1993, 1994). However, given the large (>20 μm) tortuous vessels usually found in tumors (Deane and Lantos, 1981; Pathak *et al.*, 2001), whether SE or GE methods are most appropriate remains to be determined. Several investigators have acquired relative cerebral blood volume (rCBV) maps from first-pass DSC studies, with good spatio-temporal resolution (Maeda *et al.*, 1993; Rosen *et al.*, 1991). With this technique, preliminary results indicate that MRI-derived rCBV may better differentiate histologic tumor types than conventional MRI (Aronen *et al.*, 1994) and provide information to predict tumor grade (Maeda *et al.*, 1993; Schmainda *et al.*, 2004). For a detailed description of susceptibility-based perfusion imaging of tumors see Pathak (2009).

Often MRI-derived concentration–time curves include contributions due to recirculation that must be eliminated before tumor blood volume and flow information can be extracted. This is usually accomplished by fitting to a γ-variate function with recirculation cut-off (Thompson *et al.*, 1964). For an instantaneous bolus injection of MRI contrast agent, the central volume principle states that CBF=CBV/MTT, where MTT is the mean transit time of contrast agent through the vascular network (Zierler, 1962). However, bolus injections are of finite duration, and the measured concentration–time curve is the convolution of the ideal tissue–transit curve with the AIF. Thus, measurement of the blood flow requires knowledge of the arterial input curve to deconvolve the observed concentration–time curve (Axel, 1980; Ostergaard *et al.*, 1996).

Another complication with using first-pass techniques with low molecular weight Gd contrast agents is that with elevated permeability, as is often observed in tumor vasculature or with significant blood–brain barrier (BBB) disruption, as is often the case with brain tumors, contrast agent extravasates into the brain or tumor tissue resulting in enhanced T_1 relaxation effects. In such instances, signal increases due to T_1 effects can mask signal decreases due to T_2 or T_2^* effects, leading to an underestimation of rCBV. To address this issue, a method of analysis has been devised that corrects for these leakage effects when the leakage is not extreme (Donahue *et al.*, 2000). Another obstacle to the application of the central volume principle for the calculation of blood flow is the direct measurement of the MTT. Weisskoff *et al.* have demonstrated that MTT, which relates tissue blood volume to blood flow from the central volume principle, is not the first moment of the concentration–time curve for MR of intravascular tracers, and while first moment methods cannot be used

by themselves to determine absolute flow, they do provide a useful relative measure of flow (Weisskoff, 1993).

The differential sensitivities of GE and SE methods to vessel radius have also been exploited to provide a measure of the average vessel size by measuring the ratio of GE and SE relaxation rates ($\Delta R_2^*/\Delta R_2$) (Dennie *et al.*, 1998). Donahue *et al.* (2000) demonstrated that clinically, the ratio $\Delta R_2^*/\Delta R_2$ correlated strongly with tumor grade and was a promising marker for the evaluation of tumor angiogenesis in patients.

All dynamic susceptibility-based contrast measurements are made assuming that the calibration factor that relates the relaxation rate to the contrast agent concentration is constant irrespective of tissue type. However, it has been shown that it is not the same for normal brain and tumor tissue and that this difference is due to the grossly different vascular morphology of tumors, due to tumor angiogenesis, compared to normal brain, and/or possibly differing blood rheological factors such as hematocrit (Pathak *et al.*, 2003, 2008b).

D. High molecular weight contrast agents

Quantitative assessment of tumor vascular parameters with low molecular weight contrast agents is often complicated by the rapid extravasation of the contrast agent from leaky tumor vessels. High molecular weight contrast agents, such as albumin-GdDTPA (alb-GdDTPA) complexes (Ogan *et al.*, 1987), or synthetic compounds, such as polylysine-GdDTPA (Weissleder *et al.*, 1998) and dendrimer Gd-complexes (Yu *et al.*, 2002), provide an opportunity for quantitative determination of tumor vascular volume and vascular permeability surface area product (PS). The relatively slow leakage of these agents from the vasculature results in longer circulation half-life and equilibration of plasma concentrations within the tumor. Assuming fast exchange of water between all the compartments in the tumor (plasma, interstitium, cells) the concentration of the contrast agent within any given voxel is proportional to changes in relaxation rate ($1/T_1$) before and after administration of the contrast agent. Relaxation rates can be measured either directly using fast single shot quantitative T_1 methods (Schwarzbauer *et al.*, 1993) or from T_1-weighted steady-state experiments (Brasch *et al.*, 1997), which provide better temporal resolution but are susceptible to experimental artifacts caused by variations in T_2 and T_2^* relaxation times. Pixel-wise maps can be generated from the acquired data and processed with the appropriate tracer kinetic model to obtain spatial maps of tumor vascular volume and vascular PS.

A simple linear compartment model, describing uptake of the contrast agent from plasma postulates a negligible reflux of the contrast agent from the interstitium back to the blood compartment (Fig. 1.3B). Blood concentrations of the contrast agent can be approximated to be constant for the duration of the MR experiment and under these conditions, contrast uptake can be modeled as a linear function of time (Patlak *et al.*, 1983; Roberts *et al.*, 2000). In this case, the slope of the contrast agent concentration versus time plot provides the vascular PS, and the y-intercept provides the vascular volume. For absolute values of these parameters, the change in relaxation rate of the blood must be quantified, which can be obtained separately from blood samples taken before injection of the contrast agent and at the end of the experiment, or may be obtained noninvasively (Pathak *et al.*, 2004).

Tissue concentrations of the agent over a period of up to 40 min after the bolus injection increase linearly with time. Therefore, the simple linear model is preferable for analysis of intrinsically noisy relaxation data as it is much more stable in comparison with nonlinear fitting algorithms required for the two compartment models discussed above. This linear-model approach has been employed to detect vascular differences for metastatic versus nonmetastatic breast and prostate cancer xenografts (Bhujwalla *et al.*, 2001). The accuracy of the measurement of tissue vascular volume using this approach does, however, depends on the water exchange rate between the vascular and extracellular compartments. As mentioned earlier, using a simplified model of fast exchange where there may be intermediate to slow exchange can lead to significant underestimation of vascular volume. Experimental approaches to minimize these errors are based on observations that the initial slope of the relaxation curve is independent of the exchange rate (Donahue *et al.*, 1994, 1996). Large molecular weight contrast agents have also been used to measure tumor blood flow by detecting the first pass of the agent through tumor vasculature, similar to the method described in Ostergaard *et al.* (1996), although this approach may not be feasible when the heartbeat is very rapid as in preclinical studies with rodents.

IV. IMAGING RECEPTOR EXPRESSION

The development and availability of contrast agents that generate receptor or molecular-targeted contrast has resulted in exciting new capabilities to characterize tumor vasculature and vascular targets with MRI. Mechanisms for generating MR contrast include the use of paramagnetic and superparamagnetic agents. Targeted contrast agents can be directed to cell-surface receptors expressed on tumor endothelial cells using peptides, ligands, or antibodies. These molecular imaging capabilities in combination with the strong functional imaging capabilities of MR methods will allow molecular-functional characterization of tumor vasculature.

Most of the receptor imaging studies in MRI studies of tumor angiogenesis have used imaging probes that bind to integrins such as $\alpha_v\beta_3$ (Sipkins *et al.*, 1998) and $\alpha_5\beta_1$ (Schmieder *et al.*, 2008) that are expressed on the surface of endothelial cells during neovascularization. MR contrast can be generated to image tumor angiogenesis using probes that bind to these integrins. However, MRI studies of tumor angiogenesis using targeted contrast agents are currently at the preclinical stage. A major goal for the future is to translate these preclinical developments to the clinic. The inherent low sensitivity of molecular MRI methods requires higher concentrations of MR contrast agents compared to radiopharmaceuticals and is therefore subject to more stringent Food and Drug Administration (FDA) control. The risk of nephrogenic systemic fibrosis arising from gadolinium-based contrast agents administrated to patients with kidney disease is a major concern (Neuwelt *et al.*, 2009). Recent studies have therefore focused on finding alternative MR contrast agents, such as ultrasmall superparamagnetic iron oxide (USPIO) particles, for patients at risk for nephrogenic systemic fibrosis (Neuwelt *et al.*, 2009). Unlike delivery of conventional contrast agents within the tumor interstitium where its size limits delivery, the advantage of vascular molecular imaging is that the size of the probe does not pose a delivery problem since the receptors or targets are directly accessible to the probes

circulating in the vasculature. In fact, larger sizes prolong the circulation time of the probes within the vasculature, resulting in better pharmacokinetics.

Since the RGD (Arg-Gly-Asp) peptide specifically binds to the $\alpha_v\beta_3$ integrin, USPIOs were combined with RGD peptides to visualize integrin expression through the T_2 contrast generated by the RGD–USPIOs (Zhang *et al.*, 2007). The contrast generated was found to depend on the level of $\alpha_v\beta_3$ integrin expression in different xenograft models. More recently, superparamagnetic polymeric micelles (SPPM), which consist of a cluster of SPIOs within a hydrophobic core, were used in combination with an off-resonance saturation (ORS) imaging sequence to detect $\alpha_v\beta_3$ integrin expression, as shown in Fig. 1.4. The combination of these sensitive detection probes (~70 nm in diameter) together with the ORS imaging allowed target detection within the picomolar range (Khemtong *et al.*, 2009).

Dual $\alpha_5\beta_1(\alpha_v\beta_3)$-targeted paramagnetic nanoparticles incorporating the antiangiogenic agent fumagillin were also used to create a “theranostic” agent to demonstrate the antiangiogenic effect of fumagillin with 3D MRI in preclinical studies (Schmieder *et al.*, 2008). Another colloidal iron oxide nanoparticle (CION) was also recently reported that consists of oleate-coated magnetite particles within a cross-linked phospholipid nanoemulsion (Senpan *et al.*, 2009). The sensitivity of detection reported for CION was within the nanomolar range. The outer phospholipid monolayer of the CION can be used to entrap drugs for targeted delivery to cells following membrane hemifusion. Challenges for the future will be to continue to increase the sensitivity of detection of such agents through novel chemistry, or signal amplification strategies such as hyperpolarization (Ardenkjaer-Larsen *et al.*, 2003; Day *et al.*, 2007), or instrumentation and the incorporation of multimodality imaging.

V. IMAGING VASCULAR TARGETING

Most MRI studies of vascular targeting have used functional parameters to detect changes in vasculature following the targeting. However, the great promise of noninvasive modalities such as MRI with their breadth of functional imaging capabilities is to combine molecular imaging with functional characterization, noninvasively and in vivo. The need to evaluate the efficacy of antiangiogenic and antivascular agents in vivo has created a major demand for noninvasive imaging biomarkers to individualize treatments, both in terms of matching the most suitable treatment to the patient and to determine the response to treatment (Jain *et al.*, 2009; Sorensen *et al.*, 2009). Most antiangiogenic treatments are combined with standard chemotherapy, creating a further challenge for identifying suitable noninvasive imaging biomarkers to detect the effectiveness of the antiangiogenic treatment.

Several preclinical studies have identified changes in DCE-derived parameters following antiangiogenic treatment. For example, iron oxide nanoparticle based studies have detected early vascular changes, as detected by a significant decrease of vascular volume following antiangiogenic treatment with VEGF (vascular endothelial growth factor) targeting (JuanYin *et al.*, 2009; Varallyay *et al.*, 2009). USPIOs were also used to demonstrate the antiangiogenic effects of a selective thrombogenic vascular-targeting agent consisting of the fusion peptide tTF-RGD that contains the thrombosis-inducing truncated tissue factor (tTF) together with the tumor vascular-targeting RGD peptide (Persigehl *et al.*, 2007).

Gd-based agents have also been used to assess early vascular changes following antiangiogenic treatment including VEGF targeting. Treatment with bevacizumab significantly decreased tumor vascular permeability as measured by the low molecular weight contrast agent gadodiamide (Varallyay *et al.*, 2009). The spatial heterogeneity of response to a VEGF-receptor tyrosine kinase inhibitor was evident in a study using both low and high molecular weight Gd-based contrast agents (Li *et al.*, 2005).

DCE MRI has also been used in the clinic to determine changes following antiangiogenic treatment. Most of these clinical studies have focused on the inhibition of VEGF using bevacizumab for a range of tumors such as glioblastomas (Batchelor *et al.*, 2007), rectal cancer (Willett *et al.*, 2009), and hepatocellular carcinoma (Zhu *et al.*, 2008). While a decrease of DCE-parameters was detected following treatment, additional studies are required to develop DCE MRI parameters as biomarkers to predict and detect response to antiangiogenic treatment (Jain *et al.*, 2009).

In addition to antiangiogenic agents, MRI is useful for detecting the effects of standard chemotherapeutic agents as well as novel molecular targeting agents on tumor vasculature. An increase in tumor permeability was detected using DCE MRI following TGF-β type 1 receptor inhibition (Minowa *et al.*, 2009). In this study, liposomal-GdDTPA (~120 nm size) was used as a macromolecular contrast agent that reported increased permeability following TGF-β inhibition. Liposomes are also used as carriers of anticancer drugs or molecular-based therapeutic agents such as small interfering RNA (siRNA). Decorating the liposomal membrane with MRI reporters has also been used to visualize the delivery of these carriers containing siRNA to tumors (Mikhaylova *et al.*, 2009). Image-guided tumor vascular specific delivery of MRI-detectable liposomes carrying therapeutic cargo as “theranostic agents” may be achieved by targeting the liposomes using peptides or antibodies that are specific to tumor vasculature (Torchilin, 2005).

VI. MULTIMODAL MOLECULAR-FUNCTIONAL IMAGING OF TUMOR VASCULATURE

The ultimate goal of noninvasive imaging is to be able to image a specific genetic or molecular alteration and its effects on downstream function. However, the restrictions imposed by the low sensitivity of MR detection of contrast agents (~0.1 mM) limit the detection of receptors and molecular targets that are present at low concentrations (Artemov *et al.*, 2004). Therefore, achieving molecular-functional imaging capabilities will require combining the strengths of MRI with the high sensitivity of complementary imaging modalities such as optical imaging for preclinical studies, and nuclear imaging for clinical applications. Indeed, several examples of preclinical and clinical research studies are providing exciting glimpses of the promise of multimodality imaging in understanding, characterizing, and targeting tumor angiogenesis. Advances in multimodality imaging are occurring at the level of novel multimodal probe development as well in the development of new imaging instrumentation capable of acquiring colocalized multimodal images. Several studies have already incorporated image segmentation and the landmark-based image fusion for images acquired from separate modalities. Image fusion of [$_{18}$F] Galacto-RGD PET

images with MRI using anatomical landmarks revealed good correlation between immunohistochemical distribution of $\alpha_v\beta_3$ expression and PET image intensity in human squamous cell carcinoma of the head and neck (Beer *et al.*, 2007). Regions of increased contrast uptake were identified in tumor subvolumes, demonstrating the feasibility of relating molecular expression to function with combined PET/MRI (Fig. 1.5).

In a preclinical study, VEGFR2 targeted microbubbles were used for contrast-enhanced ultrasound and correlated with DCE MRI parameters. While no discernible patterns between VEGFR2 expression and K_{trans} were evident, these studies demonstrate the feasibility of molecular-functional vascular imaging (Loveless *et al.*, 2009). Multimodal probes that can be used in combination with two or more imaging modalities are also being developed. Recently high-resolution SPECT–CT/MRI of angiogenesis in a Vx2 rabbit tumor model was reported using probes that consisted of $\alpha_v\beta_3$-targeted 99mTc nanoparticles (Lijowski *et al.*, 2009).

MRI can also be integrated with magnetic resonance spectroscopy (MRS) and magnetic resonance spectroscopic imaging (MRSI) to understand the relationship between tumor vasculature and pH or metabolism (Bhujwalla *et al.*, 2002; Provent *et al.*, 2007). In preclinical studies, multimodal approaches combining optical imaging of reporters driven by specific molecular pathways or conditions can be integrated with MRI to understand the relationship between molecular conditions such as hypoxia, or specific pathways and tumor angiogenesis and vascularization. We have used combined MRI, MRSI, and optical imaging, to study a prostate cancer model, which expresses enhanced green fluorescent protein (EGFP) under hypoxia (Raman *et al.*, 2006). In this study, a multiparametric approach of combined vascular and optical imaging was used to obtain vascular and hypoxia maps, from colocalized regions within a tumor (Raman *et al.*, 2006). In this tumor model, hypoxic regions were found to exhibit low vascular volume and high permeability. More recently a combined vascular MRI, metabolic MRSI, and optical characterization of the same tumor model identified a combination of vascular, metabolic, and hypoxic conditions that characterize metastasis-permissive environments (Penet *et al.*, 2009).

VII. CONCLUSION

MRI is continuing to evolve as an important modality for the molecular-functional characterization of the tumor vasculature. Despite the initial promise of antiangiogenic agents to effectively treat cancer, in reality, the success of these agents has been limited, due in part to the inability to stratify patients for the appropriate targeted therapies. As noninvasive molecular imaging methods develop, these will play an important role in patient selection and “personalization” of therapy.

Stem cells and endothelial progenitor cells are increasingly being implicated in tumor vascularization and the failure of antiangiogenic treatment (Monzani and La Porta, 2008; van der Schaft *et al.*, 2004). Imaging of MRI reporter-labeled stem cells or endothelial progenitor cells will provide new insights into their role in tumor angiogenesis.

Major advances are also being made in the identification of tumor vascular specific receptors (Lewis *et al.*, 2009) and through phage display (Driessen *et al.*, 2009; Kolonin *et al.*, 2001). The availability of highly specific tumor vascular markers opens avenues for image-guided targeting of the tumor angiogenesis using nanodevices that deliver therapeutic agents, gene delivery, or prodrug enzymes. With exciting developments in siRNA technology, the image-guided delivery of siRNA to tumor vasculature, visualization of this delivery via liposome technology or other nanocarriers, and detection of a therapeutic response are well within the realm of current imaging capabilities. A major direction for the future will also be to translate preclinical discoveries for use in the clinic. The availability of multimodality imaging systems that combine the strengths and capabilities of each modality should facilitate this translation.

Acknowledgments

Support from P50 CA103175, R01 CA73850, R01 CA82337, R01 CA136576, R01 CA138515, R01 CA138264, R21 CA140904, R21 CA133600, R21 CA128793 (APP), and KG090640 (APP) is gratefully acknowledged.

References

Abramovitch R, Dafni H, Smouha E, Benjamin L, Neeman M. In vivo prediction of vascular susceptibility to vascular endothelial growth factor withdrawal: Magnetic resonance imaging of C6 rat glioma in nude mice. Cancer Res. 1999; 59:5012–5016. [PubMed: 10519416]

Ardenkjaer-Larsen JH, Fridlund B, Gram A, Hansson G, Hansson L, Lerche MH, Servin R, Thaning M, Golman K. Increase in signal-to-noise ratio of >10,000 times in liquid-state NMR. Proc. Natl. Acad. Sci. USA. 2003; 100(18):10158–10163. [PubMed: 12930897]

Aronen HJ, Cohen MS, Belliveau JW, Fordham JA, Rosen BR. Ultrafast imaging of brain tumors. Top. Magn. Reson. Imaging. 1993; 5(1):14–24. [PubMed: 8416685]

Aronen HJ, Gazit IE, Louis DN, Buchbinder BR, Pardo FS, Weisskoff RM, Harsh GR, Cosgrove GR, Halpern EF, Hochberg FH, Rosen BR. Cerebral blood volume maps of gliomas: Comparison with tumor grade and histological findings. Radiology. 1994; 191:41–51. [PubMed: 8134596]

Artemov D, Bhujwalla ZM, Bulte JW. Magnetic resonance imaging of cell surface receptors using targeted contrast agents. Curr. Pharm. Biotechnol. 2004; 5(6):485–494. [PubMed: 15579038]

Axel L. Cerebral blood flow determination by rapid-sequence computed tomography: Theoretical analysis. Radiology. 1980; 137(3):679–686. [PubMed: 7003648]

Baar J, Silverman P, Lyons J, Fu P, Abdul-Karim F, Ziats N, Wasman J, Hartman P, Jesberger J, Dumadag L, Hohler E, Leeming R, et al. A vasculature-targeting regimen of preoperative docetaxel with or without bevacizumab for locally advanced breast cancer: impact on angiogenic biomarkers. Clin. Cancer Res. 2009; 15(10):3583–3590. [PubMed: 19417018]

Baluk P, Hashizume H, McDonald DM. Cellular abnormalities of blood vessels as targets in cancer. Curr. Opin. Genet. Dev. 2005; 15(1):102–111. [PubMed: 15661540]

Batchelor TT, Sorensen AG, di Tomaso E, Zhang WT, Duda DG, Cohen KS, Kozak KR, Cahill DP, Chen PJ, Zhu M, Ancukiewicz M, Mrugala MM, et al. AZD2171, a pan-VEGF receptor tyrosine kinase inhibitor, normalizes tumor vasculature and alleviates edema in glioblastoma patients. Cancer Cell. 2007; 11(1):83–95. [PubMed: 17222792]

Beer AJ, Grosu AL, Carlsen J, Kolk A, Sarbia M, Stangier I, Watzlowik P, Wester HJ, Haubner R, Schwaiger M. [^{18}F]galacto-RGD positron emission tomography for imaging of alphavbeta3 expression on the neovasculature in patients with squamous cell carcinoma of the head and neck. Clin. Cancer Res. 2007; 13(22 Pt 1):6610–6616. [PubMed: 18006761]

Bertout JA, Patel SA, Simon MC. The impact of O2 availability on human cancer. Nat. Rev. Cancer. 2008; 8(12):967–975. [PubMed: 18987634]

Bhujwalla ZM, Artemov D, Ballesteros P, Cerdan S, Gillies RJ, Solaiyappan M. Combined vascular and extracellular pH imaging of solid tumors. NMR Biomed. 2002; 15(2):114–119. [PubMed: 11870907]

Bhujwalla ZM, Artemov D, Natarajan K, Ackerstaff E, Solaiyappan M. Vascular differences detected by MRI for metastatic versus nonmetastatic breast and prostate cancer xenografts. Neoplasia. 2001; 3(2):143–153. [PubMed: 11420750]

Boxerman JL, Hamberg LM, Rosen BR, Weisskoff RM. MR contrast due to intravascular magnetic susceptibility perturbations. Magn. Reson. Med. 1995; 34:555–566. [PubMed: 8524024]

Brasch R, Pham C, Shames D, et al. Assessing tumor angiogenesis using macromolecular MR imaging contrast media. J. Magn. Reson. Imaging. 1997; 7:68–74. [PubMed: 9039595]

Brooks PC, Montgomery AM, Rosenfeld M, Reisfeld RA, Hu T, Klier G, Cheresh DA. Integrin alpha v beta 3 antagonists promote tumor regression by inducing apoptosis of angiogenic blood vessels. Cell. 1994; 79(7):1157–1164. [PubMed: 7528107]

Brown LF, Berse B, Jackman RW, Tognazzi K, Manseau EJ, Dvorak HF, Senger DR. Increased expression of vascular permeability factor (vascular endothelial growth factor) and its receptors in kidney and bladder carcinomas. Am. J. Pathol. 1993; 143(5):1255–1262. [PubMed: 8238242]

Burrows FJ, Derbyshire EJ, Tazzari PL, Amlot P, Gazdar AF, King SW, Letarte M, Vitetta ES, Thorpe PE. Up-regulation of endoglin on vascular endothelial cells in human solid tumors: Implications for diagnosis and therapy. Clin. Cancer Res. 1995; 1(12):1623–1634. [PubMed: 9815965]

Carmeliet P. Angiogenesis in life, disease and medicine. Nature. 2005; 438(7070):932–936. [PubMed: 16355210]

Carmeliet P, Dor Y, Herbert J-M, Fukumura D, Brusselmans K, Dewerchin M, Neeman M, Bono F, Abramovitch R, Maxwell P, Koch CJ, Ratcliffe P, et al. Role of HIF-1 in hypoxia-mediated apoptosis, cell proliferation and tumor angiogenesis. Nature. 1998; 394:485–490. [PubMed: 9697772]

Chang YS, di Tomaso E, McDonald DM, Jones R, Jain RK, Munn LL. Mosaic blood vessels in tumors: Frequency of cancer cells in contact with flowing blood. Proc. Natl. Acad. Sci. USA. 2000; 97(26):14608–14613. [PubMed: 11121063]

Clark ER, Hitschler WJ, KirbySmith HT, Rex RO, Smith JH. Generalobservations on the ingrowth of new blood vessels into standardized chambers in the rabbit's ear, and the subsequent changes in the newly grown vessels over a period of months. Anat. Rec. 1931; 50:129–167.

Corada M, Zanetta L, Orsenigo F, Breviario F, Lampugnani MG, Bernasconi S, Liao F, Hicklin DJ, Bohlen P, Dejana E. A monoclonal antibody to vascular endothelial-cadherin inhibits tumor angiogenesis without side effects on endothelial permeability. Blood. 2002; 100(3):905–911. [PubMed: 12130501]

Day SE, Kettunen MI, Gallagher FA, Hu DE, Lerche M, Wolber J, Golman K, Ardenkjaer-Larsen JH, Brindle KM. Detecting tumor response to treatment using hyperpolarized 13C magnetic resonance imaging and spectroscopy. Nat. Med. 2007; 13(11):1382–1387. [PubMed: 17965722]

Deane BR, Lantos PL. The vasculature of experimental brain tumors–Part 1: A sequential light and electron microscope study of angiogenesis. J. Neurol. Sci. 1981; 49:55–66. [PubMed: 7205320]

Dennie J, Mandeville JB, Boxerman JL, Packard SD, Rosen BR, Weisskoff RM. NMR imaging of changes in vascular morphology due to tumor angiogenesis. Magn. Reson. Med. 1998; 40:793–799. [PubMed: 9840821]

Donahue KM, Burstein D, MAnning WJ, Gray ML. Studies of Gd-DTPA relaxivity and proton exchange rates in tissue. Magn. Reson. Med. 1994; 32:66–75. [PubMed: 8084239]

Donahue KM, Krouwer HG, Rand SD, Pathak AP, Marszalkowski CS, Censky SC, Prost RW. Utility of simultaneously acquired gradient-echo and spin-echo cerebral blood volume and morphology maps in brain tumor patients. Magn. Reson. Med. 2000; 43(6):845–853. [PubMed: 10861879]

Donahue KM, Weisskoff RM, Burstein D. Water diffusion and exchange as they influence contrast enhancement. J. Magn. Reson. Imaging. 1997; 7(1):102–110. [PubMed: 9039599]

Donahue KM, Weisskoff RM, Chesler DA, Kwong KK, Bogdanov AA, Mandeville JB, Rosen BR. Improving MR quantitation of regional blood volume with intravascular T_1 contrast agents: Accuracy, precision, and water exchange. Magn. Reson. Med. 1996; 36:858–867. [PubMed: 8946351]

Driessen WH, Ozawa MG, Arap W, Pasqualini R. Ligand-directed cancer gene therapy to angiogenic vasculature. Adv. Genet. 2009; 67:103–121. [PubMed: 19914451]

Epstein AL, Khawli LA, Hornick JL, Taylor CR. Identification of a monoclonal antibody, TV-1, directed against the basement membrane of tumor vessels, and its use to enhance the delivery of macromolecules to tumors after conjugation with interleukin 2. Cancer Res. 1995; 55(12):2673–2680. [PubMed: 7780984]

Fisel CR, Ackerman JL, Buxton RB, Garrido L, Belliveau JW, Rosen RB, Brady TJ. MR contrast due to microscopically heterogeneous magnetic susceptibility: Numerical simulations and applications to cerebral physiology. Magn. Reson. Med. 1991; 17:336–347. [PubMed: 2062208]

Folkman J. Tumor angiogenesis: therapeutic implications. N. Engl. J. Med. 1971; 285(21):1182–1186. [PubMed: 4938153]

Folkman J. Angiogenesis: An organizing principle for drug discovery? Nat. Rev. Drug Discov. 2007; 6(4):273–286. [PubMed: 17396134]

Forster-Horvath C, Meszaros L, Raso E, Dome B, Ladanyi A, Morini M, Albini A, Timar J. Expression of CD44v3 protein in human endothelial cells in vitro and in tumoral microvessels in vivo. Microvasc. Res. 2004; 68(2):110–118. [PubMed: 15313120]

Glunde K, Pathak AP, Bhujwalla ZM. Molecular-functional imaging of cancer: to image and imagine. Trends Mol. Med. 2007; 13(7):287–297. [PubMed: 17544849]

Goldman E. The growth of malignant disease in man and the lower animals, with special reference to the vascular system. Proc. R. Soc. Med. 1907; 1:1–13.

Hagemeier HH, Vollmer E, Goerdt S, Schulze-Osthoff K, Sorg C. A monoclonal antibody reacting with endothelial cells of budding vessels in tumors and inflammatory tissues, and non-reactive with normal adult tissues. Int. J. Cancer. 1986; 38(4):481–488. [PubMed: 3531031]

Hallahan DE, Staba-Hogan MJ, Virudachalam S, Kolchinsky A. X-ray-induced P-selectin localization to the lumen of tumor blood vessels. Cancer Res. 1998; 58(22):5216–5220. [PubMed: 9823335]

Holash J, Maisonpierre PC, Compton D, Boland P, Alexander CR, Zagzag D, Yancopoulos GD, Wiegand SJ. Vessel cooption, regression, and growth in tumors mediated by angiopoietins and VEGF. Science. 1999; 284(5422):1994–1998. [PubMed: 10373119]

Hunter, J. Treatise on the blood, inflammation and gunshot wounds. Thomas Bradford; Phildelphia: 1794.

Jain RK. Determinants of tumor blood flow: A review. Cancer Res. 1988; 48(10):2641–2658. [PubMed: 3282647]

Jain RK, Carmeliet PF. Vessels of death or life. Sci. Am. 2001; 285(6):38–45. [PubMed: 11759584]

Jain RK, Duda DG, Willett CG, Sahani DV, Zhu AX, Loeffler JS, Batchelor TT, Sorensen AG. Biomarkers of response and resistance to antiangiogenic therapy. Nat. Rev. Clin. Oncol. 2009; 6(6):327–338. [PubMed: 19483739]

Jarnum H, Steffensen EG, Knutsson L, Frund ET, Simonsen CW, Lundbye-Christensen S, Shankaranarayanan A, Alsop DC, Jensen FT, Larsson EM. Perfusion MRI of brain tumours: a comparative study of pseudo-continuous arterial spin labelling and dynamic susceptibility contrast imaging. Neuroradiology. 2010; 52(4):307–317. [PubMed: 19841916]

JuanYin J, Tracy K, Zhang L, Munasinghe J, Shapiro E, Koretsky A, Kelly K. Noninvasive imaging of the functional effects of anti-VEGF therapy on tumor cell extravasation and regional blood volume in an experimental brain metastasis model. Clin. Exp. Metastasis. 2009; 26(5):403–414. [PubMed: 19277878]

Kalluri R. Basement membranes: Structure, assembly and role in tumour angiogenesis. Nat. Rev. Cancer. 2003; 3(6):422–433. [PubMed: 12778132]

Karumanchi SA, Jha V, Ramchandran R, Karihaloo A, Tsiokas L, Chan B, Dhanabal M, Hanai JI, Venkataraman G, Shriver Z, Keiser N, Kalluri R, et al. Cell surface glypicans are low-affinity endostatin receptors. Mol. Cell. 2001; 7(4):811–822. [PubMed: 11336704]

Kennan RP. Intravascular susceptibility contrast mechanisms in tissues. Magn. Reson. Med. 1994; 31:9–21. [PubMed: 8121277]

Khemtong C, Kessinger CW, Ren J, Bey EA, Yang SG, Guthi JS, Boothman DA, Sherry AD, Gao J. In vivo off-resonance saturation magnetic resonance imaging of alphavbeta3-targeted superparamagnetic nanoparticles. Cancer Res. 2009; 69(4):1651–1658. [PubMed: 19190328]

Kim YR, Rebro KJ, Schmainda KM. Water exchange and inflow affect the accuracy of T_1-GRE blood volume measurements: Implications for the evaluation of tumor angiogenesis. Magn. Reson. Med. 2002; 47(6):1110–1120. [PubMed: 12111957]

Knutsson L, van Westen D, Petersen ET, Bloch KM, Holtas S, Stahlberg F, Wirestam R. Absolute quantification of cerebral blood flow: correlation between dynamic susceptibility contrast MRI and model-free arterial spin labeling. Magn. Reson. Imaging. 2010; 28(1):1–7. [PubMed: 19695822]

Koivunen E, Arap W, Valtanen H, Rainisalo A, Medina OP, Heikkila P, Kantor C, Gahmberg CG, Salo T, Konttinen YT, Sorsa T, Ruoslahti E, et al. Tumor targeting with a selective gelatinase inhibitor. Nat. Biotechnol. 1999; 17(8):768–774. [PubMed: 10429241]

Kolonin M, Pasqualini R, Arap W. Molecular addresses in blood vessels as targets for therapy. Curr. Opin. Chem. Biol. 2001; 5(3):308–313. [PubMed: 11479123]

Konerding, MA.; van Ackern, C.; Fait, E.; Steinberg, F.; Streffer, C. Blood Perfusion and Microenvironment of Human Tumors: Implications for Clinical Radiooncology. Springer. Verlag; New York: 2000. Morphological aspects of tumor angiogenesis and microcirculation; p. 5-17.

Landis CS, Li X, Telang FW, Coderre JA, Micca PL, Rooney WD, Latour LL, Vetek G, Palyka I, Springer CS Jr. Determination of the MRI contrast agent concentration time course in vivo following bolus injection: Effect of equilibrium transcytolemmal water exchange. Magn. Reson. Med. 2000; 44(4):563–574. [PubMed: 11025512]

Langenkamp E, Molema G. Microvascular endothelial cell heterogeneity: General concepts and pharmacological consequences for anti-angiogenic therapy of cancer. Cell Tissue Res. 2009; 335(1):205–222. [PubMed: 18677515]

Lauffer RB. Paramagnetic metal complexes as water proton relaxation agents for NMR imaging: Theory and design. Chem. Rev. 1987; 87:901–927.

Lewis VO, Ozawa MG, Deavers MT, Wang G, Shintani T, Arap W, Pasqualini R. The interleukin-11 receptor alpha as a candidate ligand-directed target in osteosarcoma: Consistent data from cell lines, orthotopic models, and human tumor samples. Cancer Res. 2009; 69(5):1995–1999. [PubMed: 19244100]

Lewis W. The vascular patterns of tumors. Bull. Johns Hopkins Hosp. 1927; 41:156–162.

Li KL, Wilmes LJ, Henry RG, Pallavicini MG, Park JW, Hu-Lowe DD, McShane TM, Shalinsky DR, Fu YJ, Brasch RC, Hylton NM. Heterogeneity in the angiogenic response of a BT474 human breast cancer to a novel vascular endothelial growth factor-receptor tyrosine kinase inhibitor: Assessment by voxel analysis of dynamic contrast-enhanced MRI. J. Magn. Reson. Imaging. 2005; 22(4):511–519. [PubMed: 16161072]

Lijowski M, Caruthers S, Hu G, Zhang H, Scott MJ, Williams T, Erpelding T, Schmieder AH, Kiefer G, Gulyas G, Athey PS, Gaffney PJ, et al. High sensitivity: High-resolution SPECT-CT/MR molecular imaging of angiogenesis in the Vx2 model. Invest. Radiol. 2009; 44(1):15–22. [PubMed: 18836386]

Loveless ME, Whisenant JG, Wilson K, Lyshchik A, Sinha TK, Gore JC, Yankeelov TE. Coregistration of ultrasonography and magnetic resonance imaging with a preliminary investigation of the spatial colocalization of vascular endothelial growth factor receptor 2 expression and tumor perfusion in a murine tumor model. Mol. Imaging. 2009; 8(4):187–198. [PubMed: 19728973]

Maeda M, Itoh S, Kimura H, Iwasaki T, Hayashi N, Yamamoto K, Ishii Y, Kubota T. Tumor vascularity in the brain: Evaluation with dynamic susceptibility-contrast MR imaging. Radiology. 1993; 189:233–238. [PubMed: 8372199]

Maniotis AJ, Folberg R, Hess A, Seftor EA, Gardner LM, Pe'er J, Trent JM, Meltzer PS, Hendrix MJ. Vascular channel formation by human melanoma cells in vivo and in vitro: Vasculogenic mimicry. Am. J. Pathol. 1999; 155(3):739–752. [PubMed: 10487832]

Mayr NA, Yuh WT, Jajoura D, Wang JZ, Lo SS, Montebello JF, Porter K, Zhang D, McMeekin DS, Buatti JM. Ultra-early predictive assay for treatment failure using functional magnetic resonance imaging and clinical prognostic parameters in cervical cancer. Cancer. 2010; 116(4):903–912. [PubMed: 20052727]

McDonald DM, Choyke PL. Imaging of angiogenesis: From microscope to clinic. Nat. Med. 2003; 9(6):713–725. [PubMed: 12778170]

Mikhaylova M, Stasinopoulos I, Kato Y, Artemov D, Bhujwalla ZM. Imaging of cationic multifunctional liposome-mediated delivery of COX-2 siRNA. Cancer Gene Ther. 2009; 16(3): 217–226. [PubMed: 18927599]

Minowa T, Kawano K, Kuribayashi H, Shiraishi K, Sugino T, Hattori Y, Yokoyama M, Maitani Y. Increase in tumour permeability following TGF-β type I receptor-inhibitor treatment observed by dynamic contrast-enhanced MRI. Br. J. Cancer. 2009; 101(11):1884–1890. [PubMed: 19888220]

Molema G. Design of vascular endothelium-specific drug-targeting strategies for the treatment of cancer. Acta Biochim. Pol. 2005; 52(2):301–310. [PubMed: 15990916]

Molls, M.; Vaupel, P. The impact of the tumor microenvironment on experimental and clinical radiation oncology and other therapeutic modalities. In: Brady, LW.; Heilman, H-P.; Molls, M., editors. In “Blood Perfusion and Microenvironment of Human Tumors: Implications for Clinical Radiooncology”. Springer Verlag; New York: 2000. p. 1-4.

Monzani E, La Porta CA. Targeting cancer stem cells to modulate alternative vascularization mechanisms. Stem Cell Rev. 2008; 4(1):51–56. [PubMed: 18286393]

Moser TL, Stack MS, Asplin I, Enghild JJ, Hojrup P, Everitt L, Hubchak S, Schnaper HW, Pizzo SV. Angiostatin binds ATP synthase on the surface of human endothelial cells. Proc. Natl. Acad. Sci. USA. 1999; 96(6):2811–2816. [PubMed: 10077593]

Munn LL. Aberrant vascular architecture in tumors and its importance in drug-based therapies. Drug Discov. Today. 2003; 8(9):396–403. [PubMed: 12706657]

Neri D, Bicknell R. Tumour vascular targeting. Nat. Rev. Cancer. 2005; 5(6):436–446. [PubMed: 15928674]

Neuwelt EA, Hamilton BE, Varallyay CG, Rooney WR, Edelman RD, Jacobs PM, Watnick SG. Ultrasmall superparamagnetic iron oxides (USPIOs): A future alternative magnetic resonance (MR) contrast agent for patients at risk for nephrogenic systemic fibrosis (NSF)? Kidney Int. 2009; 75(5):465–474. [PubMed: 18843256]

Nguyen M, Strubel NA, Bischoff J. A role for sialyl Lewis-X/A glycoconjugates in capillary morphogenesis. Nature. 1993; 365(6443):267–269. [PubMed: 7690465]

Ogan MD, Schmiedl U, Mosley ME, Grodd W, Paajanen H, Brasch RC. Albumin labeled with Gd-DTPA; an intravascular contrast enhancing agent for magnetic resonance blood pool imaging: Preparation and characterization. Invest. Radiol. 1987; 22:665–671. [PubMed: 3667174]

Ogawa S. Oxygenation-sensitive contrast in MR image of rodent brain at high magnetic fields. Magn. Reson. Med. 1990; 14:68–78. [PubMed: 2161986]

Oh P, Li Y, Yu J, Durr E, Krasinska KM, Carver LA, Testa JE, Schnitzer JE. Subtractive proteomic mapping of the endothelial surface in lung and solid tumours for tissue-specific therapy. Nature. 2004; 429(6992):629–635. [PubMed: 15190345]

Ohno KP, Pettigrew KD, Rapoport SI. Local cerebral blood flow in the conscious rat as measured with 14C-antipyrine, 14C-iodoantipyrine and 3H-nicotine. Stroke. 1979; 10(1):62–67. [PubMed: 432901]

Ostergaard L, Weisskoff RM, Chesler DA, Gyldensted C, Rosen BR. High resolution measurement of cerebral blood flow using intravascular tracer bolus passages. Part I: Mathematical approach and statistical analysis. Magn. Reson. Med. 1996; 36(5):715–725. [PubMed: 8916022]

Pasqualini R, Koivunen E, Kain R, Lahdenranta J, Sakamoto M, Stryhn A, Ashmun RA, Shapiro LH, Arap W, Ruoslahti E. Aminopeptidase N is a receptor for tumor-homing peptides and a target for inhibiting angiogenesis. Cancer Res. 2000; 60(3):722–727. [PubMed: 10676659]

Pathak AP. Magnetic resonance susceptibility based perfusion imaging of tumors using iron oxide nanoparticles. Wiley Interdiscip. Rev. Nanomed. Nanobiotechnol. 2009; 1(1):84–97. [PubMed: 20049781]

Pathak AP, Artemov D, Bhujwalla ZB. A novel system for determining contrast agent concentration in mouse blood in vivo. Magn. Reson. Med. 2004; 51(3):612–615. [PubMed: 15004805]

Pathak AP, Hochfeld WE, Goodman SL, Pepper MS. Circulating and imaging markers for angiogenesis. Angiogenesis. 2008a; 11(4):321–335. [PubMed: 18925424]

Pathak AP, Rand SD, Schmainda KM. The effect of brain tumor angiogenesis on the in vivo relationship between the gradient echo relaxation rate change (DR2*) and contrast agent (MION) dose. J. Magn. Reson. Imaging. 2003; 18(4):397–403. [PubMed: 14508775]

Pathak AP, Schmainda KM, Ward BD, Linderman JR, Rebro KJ, Greene AS. MR-derived cerebral blood volume maps: Issues regarding histological validation and assessment of tumor angiogenesis. Magn. Reson. Med. 2001; 46(4):735–747. [PubMed: 11590650]

Pathak AP, Ward BD, Schmainda KM. A novel technique for modeling susceptibility-based contrast mechanisms for arbitrary microvascular geometries: The finite perturber method. Neuroimage. 2008b; 40(3):1130–1143. [PubMed: 18308587]

Patlak CS, Blasberg RG, Fenstermacher JD. Graphical evaluation of blood-to-brain transfer constants from multiple-time uptake data. J. Cereb. Blood Flow Metab. 1983; 3:1–7. [PubMed: 6822610]

Penet MF, Pathak AP, Raman V, Ballesteros P, Artemov D, Bhujwalla ZM. Noninvasive multiparametric imaging of metastasis-permissive microenvironments in a human prostate cancer xenograft. Cancer Res. 2009; 69(22):8822–8829. [PubMed: 19861534]

Persigehl T, Bieker R, Matuszewski L, Wall A, Kessler T, Kooijman H, Meier N, Ebert W, Berdel WE, Heindel W, Mesters RM, Bremer C. Antiangiogenic tumor treatment: Early noninvasive monitoring with USPIO-enhanced MR imaging in mice. Radiology. 2007; 244(2):449–456. [PubMed: 17562810]

Provent P, Benito M, Hiba B, Farion R, Lopez-Larrubia P, Ballesteros P, Remy C, Segebarth C, Cerdan S, Coles JA, Garcia-Martin ML. Serial in vivo spectroscopic nuclear magnetic resonance imaging of lactate and extracellular pH in rat gliomas shows redistribution of protons away from sites of glycolysis. Cancer Res. 2007; 67(16):7638–7645. [PubMed: 17699768]

Raman V, Artemov D, Pathak AP, Winnard PT Jr. McNutt S, Yudina A, Bogdanov A Jr. Bhujwalla ZM. Characterizing vascular parameters in hypoxic regions: A combined magnetic resonance and optical imaging study of a human prostate cancer model. Cancer Res. 2006; 66(20):9929–9936. [PubMed: 17047055]

Rettig WJ, Garin-Chesa P, Healey JH, Su SL, Jaffe EA, Old LJ. Identification of endosialin, a cell surface glycoprotein of vascular endothelial cells in human cancer. Proc. Natl. Acad. Sci. USA. 1992; 89(22):10832–10836. [PubMed: 1438285]

Ribatti, D. Early evidence of the vascular phase and its importance in tumor growth. In: Ribatti, D., editor. In “History of Research on Tumor Angiogenesis”. Springer; Netherlands: 2009. p. 1-17.

Roberts HC, Roberts RC, Brasch RT, Dillon WP. Quantitative measurement of microvascular permeability in human brain tumors achieved using dynamic contrast-enhanced MR imaging: Correlation with histologic grade. AJNR Am J Neuroradiol. 2000; 21(5):891–899. [PubMed: 10815665]

Rosen BR, Belliveau JW, Buchbinder BR, McKinstry RC, Porkka LM, Kennedy DN, Neuder MS, Fisel CR, Aronen HJ, Kwong KK, Weisskoff RM, Cohen MS, et al. Contrast agents and cerebral hemodynamics. Magn. Reson. Med. 1991; 19:285–292. [PubMed: 1881317]

Sato TN, Tozawa Y, Deutsch U, Wolburg-Buchholz K, Fujiwara Y, Gendron-Maguire M, Gridley T, Wolburg H, Risau W, Qin Y. Distinct roles of the receptor tyrosine kinases Tie-1 and Tie-2 in blood vessel formation. Nature. 1995; 376(6535):70–74. [PubMed: 7596437]

Schlingemann RO, Rietveld FJ, de Waal RM, Bradley NJ, Skene AI, Davies AJ, Greaves MF, Denekamp J, Ruiter DJ. Leukocyte antigen CD34 is expressed by a subset of cultured endothelial cells and on endothelial abluminal microprocesses in the tumor stroma. Lab. Invest. 1990; 62(6): 690–696. [PubMed: 1694254]

Schmainda KM, Rand SD, Joseph AM, Lund R, Ward BD, Pathak AP, Ulmer JL, Badruddoja MA, Krouwer HG. Characterization of a first-pass gradient-echo spin-echo method to predict brain tumor grade and angiogenesis. AJNR Am. J. Neuroradiol. 2004; 25(9):1524–1532. [PubMed: 15502131]

Schmieder AH, Caruthers SD, Zhang H, Williams TA, Robertson JD, Wickline SA, Lanza GM. Three-dimensional MR mapping of angiogenesis with alpha5beta1 (alpha nu beta3)-targeted theranostic nanoparticles in the MDA-MB-435 xenograft mouse model. FASEB J. 2008; 22(12):4179–4189. [PubMed: 18697838]

Schwarzbauer C, Syha J, Haase A. Quantification of regional cerebral blood volumes by rapid T_1 mapping. Magn. Reson. Med. 1993; 29:709–712. [PubMed: 8505910]

Semenza GL. Defining the role of hypoxia-inducible factor 1 in cancer biology and therapeutics. Oncogene. 2010; 29(5):625–634. [PubMed: 19946328]

Senpan A, Caruthers SD, Rhee I, Mauro NA, Pan D, Hu G, Scott MJ, Fuhrhop RW, Gaffney PJ, Wickline SA, Lanza GM. Conquering the dark side: Colloidal iron oxide nanoparticles. ACS Nano. 2009; 3(12):3917–3926. [PubMed: 19908850]

Silva AC, Kim S-G, Garwood M. Imaging blood flow in brain tumors using arterial spin labeling. Magn. Reson. Med. 2000; 44:169–173. [PubMed: 10918313]

Sipkins DA, Cheresh DA, Kazemi MR, Nevin LM, Bednarski MD, Li KC. Detection of tumor angiogenesis in vivo by alphaVbeta3-targeted magnetic resonance imaging. Nat. Med. 1998; 4(5):623–626. [PubMed: 9585240]

Sorensen AG, Batchelor TT, Zhang WT, Chen PJ, Yeo P, Wang M, Jennings D, Wen PY, Lahdenranta J, Ancukiewicz M, di Tomaso E, Duda DG, et al. A “vascular normalization index” as potential mechanistic biomarker to predict survival after a single dose of cediranib in recurrent glioblastoma patients. Cancer Res. 2009; 69(13):5296–5300. [PubMed: 19549889]

Croix B, St, Rago C, Velculescu V, Traverso G, Romans KE, Montgomery E, Lal A, Riggins GJ, Lengauer C, Vogelstein B, Kinzler KW. Genes expressed in human tumor endothelium. Science. 2000; 289(5482):1197–1202. [PubMed: 10947988]

Tarli L, Balza E, Viti F, Borsi L, Castellani P, Berndorff D, Dinkelborg L, Neri D, Zardi L. A high-affinity human antibody that targets tumoral blood vessels. Blood. 1999; 94(1):192–198. [PubMed: 10381513]

Thomlinson RH, Gray LH. The histological structure of some human lung cancers and the possible implications for radiotherapy. Br. J. Cancer. 1955; 9(4):539–549. [PubMed: 13304213]

Thompson HKJ, Starmer CF, Whalen RE, McIntosh HD. Indicator transit time considered as a gamma-variate. Circulation Res. Jun.1964 XIV

Tofts PS. Modeling tracer kinetics in dynamic Gd-DTPA MR imaging. J. Magn. Reson. Imaging. 1997; 7(1):91–101. [PubMed: 9039598]

Tofts PS, Brix G, Evelhoch JL, Buckley DL, Henderson E, Larsson HB, Knopp MV, Lee TY, Parker GJ, Mayr NA, Taylor J, Port RE, et al. Estimating kinetic parameters from dynamic contrast-enhanced T(1)-weighted MRI of a diffusable tracer: Standardized quantities and symbols. J. Magn. Reson. Imaging. 1999; 10(3):223–232. [PubMed: 10508281]

Torchilin VP. Recent advances with liposomes as pharmaceutical carriers. Nat. Rev. Drug Discov. 2005; 4(2):145–160. [PubMed: 15688077]

van der Schaft DW, Seftor RE, Seftor EA, Hess AR, Gruman LM, Kirschmann DA, Yokoyama Y, Griffioen AW, Hendrix MJ. Effects of angiogenesis inhibitors on vascular network formation by human endothelial and melanoma cells. J. Natl. Cancer Inst. 2004; 96(19):1473–1477. [PubMed: 15467037]

Varallyay CG, Muldoon LL, Gahramanov S, Wu YJ, Goodman JA, Li X, Pike MM, Neuwelt EA. Dynamic MRI using iron oxide nanoparticles to assess early vascular effects of antiangiogenic versus corticosteroid treatment in a glioma model. J. Cereb. Blood Flow Metab. 2009; 29(4):853–860. [PubMed: 19142191]

Vaupel P, Kallinowski F, Okunieff P. Blood flow, oxygen and nutrient supply, and metabolic microenvironment of human tumors: A review. Cancer Res. 1989; 49(23):6449–6465. [PubMed: 2684393]

Villringer A, Rosen BR, Belliveau JW, Ackerman JL, Lauffer RB, Buxton RB, Chao YS, Wedeen VJ, Brady TJ. Dynamic imaging with lanthanide chelates in normal brain: Contrast due to magnetic susceptibility effects. Magn. Reson. Med. 1988; 6:164–174. [PubMed: 3367774]

Virchow, R. Die krankhaften Geschwultste. Hirschwald, Berlin: 1863.

Weisskoff RM. Pitfalls in MR measurement of tissue blood flow with intravascular tracers: Which mean transit time. Magn. Reson. Med. 1993; 29:553–559. [PubMed: 8464373]

Weisskoff RM, Zuo CS, Boxerman JL, Rosen BR. Microscopic susceptibility variation and transverse relaxation: Theory and experiment. Magn. Reson. Med. 1994; 31:601–610. [PubMed: 8057812]

Weissleder R, Cheng HC, Marecos E, Kwong K, Bogdanov A Jr. Non-invasive in vivo mapping of tumour vascular and interstitial volume fractions. Eur. J. Cancer. 1998; 34(9):1448–1454. [PubMed: 9849430]

Willett CG, Duda DG, di Tomaso E, Boucher Y, Ancukiewicz M, Sahani DV, Lahdenranta J, Chung DC, Fischman AJ, Lauwers GY, Shellito P, Czito BG, et al. Efficacy, safety, and biomarkers of

neoadjuvant bevacizumab, radiation therapy, and fluorouracil in rectal cancer: A multidisciplinary phase II study. J. Clin. Oncol. 2009; 27(18):3020–3026. [PubMed: 19470921]

Yablonskiy DA. Theory of NMR signal behavior in magnetically inhomogeneous tissues: The static dephasing regime. Magn. Reson. Med. 1994; 32:749–763. [PubMed: 7869897]

Yu H, Su MY, Wang Z, Nalcioglu O. A longitudinal study of radiation-induced changes in tumor vasculature by contrast-enhanced magnetic resonance imaging. Radiat. Res. 2002; 158(2):152–158. [PubMed: 12105984]

Zaharchuk G. Theoretical basis of hemodynamic MR imaging techniques to measure cerebral blood volume, cerebral blood flow, and permeability. AJNR Am. J. Neuroradiol. 2007; 28(10):1850–1858. [PubMed: 17998415]

Zhang C, Jugold M, Woenne EC, Lammers T, Morgenstern B, Mueller MM, Zentgraf H, Bock M, Eisenhut M, Semmler W, Kiessling F. Specific targeting of tumor angiogenesis by RGD-conjugated ultrasmall superparamagnetic iron oxide particles using a clinical 1.5-T magnetic resonance scanner. Cancer Res. 2007; 67(4):1555–1562. [PubMed: 17308094]

Zhao D, Jiang L, Hahn EW, Mason RP. Comparison of 1H blood oxygen level-dependent (BOLD) and 19F MRI to investigate tumor oxygenation. Magn. Reson. Med. 2009; 62(2):357–364. [PubMed: 19526495]

Zhu AX, Holalkere NS, Muzikansky A, Horgan K, Sahani DV. Early antiangiogenic activity of bevacizumab evaluated by computed tomography perfusion scan in patients with advanced hepatocellular carcinoma. Oncologist. 2008; 13(2):120–125. [PubMed: 18305056]

Zierler KL. Theoretical basis of indicator-dilution methods for measuring flow and volume. Circulation Res. Mar.1962 X:393–407.

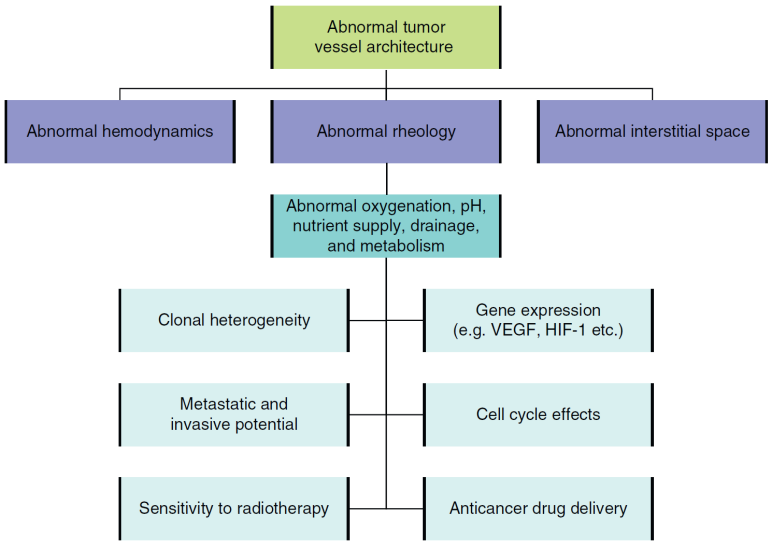

Figure 1.1.

Schematic to illustrate how abnormal tumor vessel architecture results in altered hemodynamics (blood flow), blood rheology, and elevated interstitial fluid pressure. These alterations in turn profoundly affects the tumor microenvironment (i.e., oxygenation, pH, etc.), which in turn modulates multiple phenomena ranging from gene expression to sensitivity to radiotherapy. Adapted from Molls and Vaupel (2000).

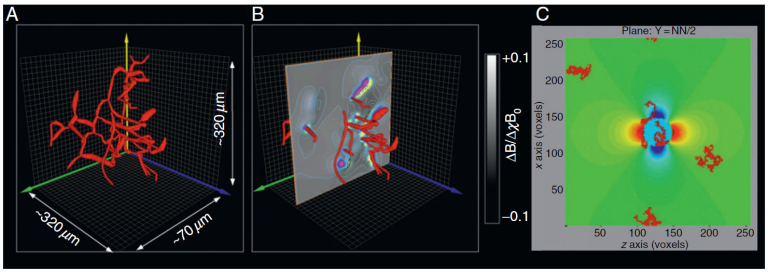

Figure 1.2.

(A) 3D volume rendering of a rat cerebrocortical capillary network. (B) Capillary network in (A) overlaid with a slice through the 3D magnetic field map showing the microscopic magnetic field heterogeneities generated by the contrast agent bearing blood vessels. (C) Projection of five 3D proton diffusion trajectories onto a slice through the 3D magnetic field perturbation due to a contrast agent bearing blood vessel cylinder for the restricted proton diffusion case, that is, protons are not allowed to traverse the vessel boundary. These data are results of numerical simulations adapted with permission from Pathak *et al.* (2008b).

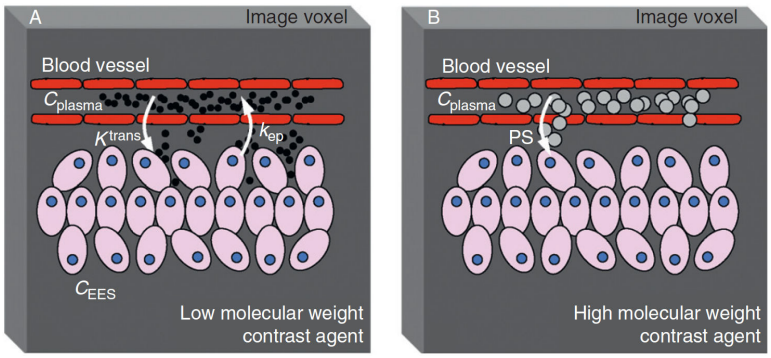

Figure 1.3.

(A) Schematic of an imaging voxel relating the exchange of a low molecular weight contrast agent (e.g., GdDTPA) postadministration between plasma and the interstitial space. The plasma volume is usually small compared to the volume of the extravascular extracellular space or EES (shown in gray) and the intercellular space (shown in blue), which is inaccessible to the contrast agent. K_{trans} is the volume transfer constant between the blood plasma and EES, while kep is the rate constant between the EES and blood plasma. (B) Schematic of an imaging voxel demonstrating conditions for a macromolecular or high molecular weight agent (e.g., albumin-GdDTPA), which exhibits relatively slow leakage from the vasculature, longer circulation half-life, and equilibration of plasma concentrations within the tumor. Postadministration, the bulk of the T1 relaxation effect is proportional to the volume of the intravascular space since the contrast agent is initially confined to this space. As the contrast agent slowly extravasates into the EES, the volume transfer constant is proportional to the permeability surface area product (PS) of the tumor vasculature.

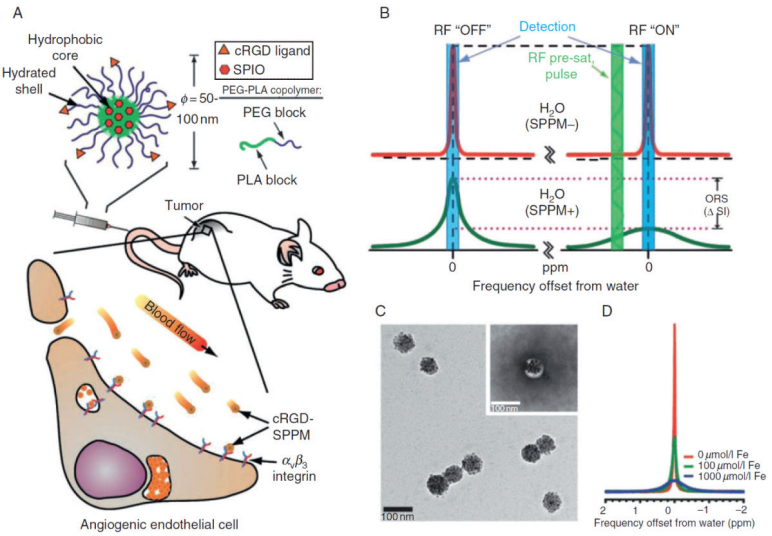

Figure 1.4.

Cancer molecular imaging by cRGD-encoded SPPM and ORS MRI. (A) Schematic illustration of a cRGD-encoded SPPM and its targeting to αvβ3-expressing endothelial cells in the tumor vasculature. (B) Mechanism of SPPM-induced ORS contrast. A presaturation RF pulse results in a significant decrease of signal intensity (ΔSI) in SPPM(+) H_2O over SPPM(−) H_2O. (C) Transmission electron microscopy (TEM) image of a representative SPPM sample. Inset, a SPPM particle after negative staining with 2% phosphotungstic acid (PTA) solution. (D) 1H NMR (300 MHz) spectra of water containing different concentrations of SPPM (in [Fe]/mmol/L). Adapted with permission from Khemtong *et al.* (2009). PEG-PLA, poly(ethylene glycol)-block-poly(d,l-lactide).

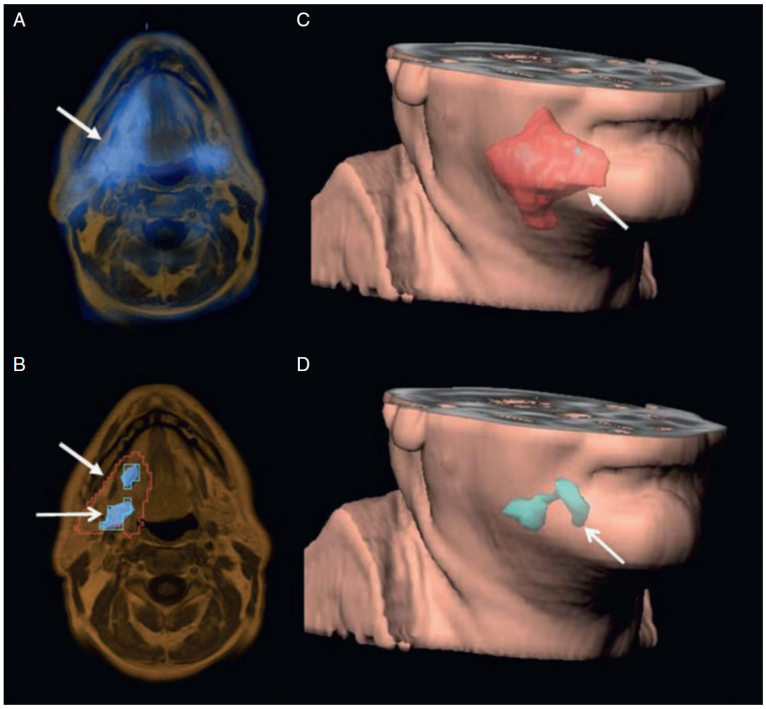

Figure 1.5.

Patient with a squamous cell carcinoma of the head and neck in the right oral cavity. The [^{18}F]Galacto-RGD PET/MRI image fusion (A) shows intense and heterogeneous tracer uptake in the lesion (arrow). Moderate uptake is also notable in the submandibular gland. A transaxial MRI slice of the tumor volume as defined by MRI (B, closed-tipped arrow; red line) and in the corresponding 3D reconstruction (C, closed-tipped arrow). By applying a threshold of standardized uptake values (SUV)=3 and only using pixels with SUVs above this threshold, a subvolume with more intense $\alpha_v\beta_3$ expression could be defined (blue line and blue area, B; open-tipped arrow), (D, blue volume; open-tipped arrow). Adapted with permission from (Beer *et al.*, 2007).

Table 1.1

Epitopes on Angiogenic Endothelial Cells and Basement Membrane Components that may serve as Targets for Tumor Vasculature-Selective Drug-Targeting Strategies

Target	References
30.5 kDa antigen	Hagemeier *et al.* (1986)
CD34	Schlingemann *et al.* (1990)
VEGF–VEGFR complex[a]	Brown *et al.* (1993)
Endosialin	Rettig *et al.* (1992)
Selectins[a]	Nguyen *et al.* (1993)
αv integrins[a]	Brooks *et al.* (1994)
Endoglin[a]	Burrows *et al.* (1995)
Tie-2	Sato *et al.* (1995)
Angiostatin receptor	Moser *et al.* (1999)
MMP-2/MMP-9[a]	Koivunen *et al.* (1999)
CD13/Aminopeptidase N[a]	Pasqualini *et al.* (2000)
Endostatin receptor	Karumanchi *et al.* (2001)
TEM 1/5/8	Croix *et al.* (2000)
VE cadherin cryptic epitope[a]	Corada *et al.* (2002)
CD44v3	Forster-Horvath *et al.* (2004)
Annexin A1	Oh *et al.* (2004)
Inducible target	
P-selectin	Hallahan *et al.* (1998)
Extracellular matrix target	
EDB-Fn[a]	Tarli *et al.* (1999)
Basement membrane component	Epstein *et al.* (1995)

Adapted with permission from Molema (2005).

[a]Denotes the target molecules experimentally employed for tumor vascular drug-targeting strategies. EDB-Fn, EDB-oncofetal domain of fibronectin; MMP, matrix metalloproteinase; TEM, tumor endothelial marker; VEGF(R), vascular endothelial growth factor (receptor).